THE JOURNAL OF BIOLOGICAL CHEMISTRY VOL. 291, NO. 22, pp. 11887–11898, May 27, 2016

The Structure of the Complex between Yeast Frataxin and Ferrochelatase

*CHARACTERIZATION AND PRE-STEADY STATE REACTION OF FERROUS IRON DELIVERY AND HEME SYNTHESIS**[S]

Received for publication, October 29, 2015, and in revised form, March 11, 2016 Published, JBC Papers in Press, March 29, 2016, DOI 10.1074/jbc.M115.701128

Christopher Söderberg[‡1,2], **Mallory E. Gillam**[§1], **Eva-Christina Ahlgren**[‡], **Gregory A. Hunter**[§], **Oleksandr Gakh**[¶], **Grazia Isaya**[¶], **Gloria C. Ferreira**[§‖3], **and Salam Al-Karadaghi**[‡4]

From the [‡]*Center for Molecular Protein Science, Department of Chemistry, Lund University, SE-221 00 Lund, Sweden,* [§]*Department of Molecular Medicine, Morsani College of Medicine and the* [‖]*Department of Chemistry, University of South Florida, Tampa, Florida 33612, and the* [¶]*Departments of Pediatric and Adolescent Medicine and Biochemistry and Molecular Biology, Mayo Clinic, College of Medicine, Rochester, Minnesota 55905*

Frataxin is a mitochondrial iron-binding protein involved in iron storage, detoxification, and delivery for iron sulfur-cluster assembly and heme biosynthesis. The ability of frataxin from different organisms to populate multiple oligomeric states in the presence of metal ions, *e.g.* Fe^{2+} and Co^{2+}, led to the suggestion that different oligomers contribute to the functions of frataxin. Here we report on the complex between yeast frataxin and ferrochelatase, the terminal enzyme of heme biosynthesis. Protein-protein docking and cross-linking in combination with mass spectroscopic analysis and single-particle reconstruction from negatively stained electron microscopic images were used to verify the Yfh1-ferrochelatase interactions. The model of the complex indicates that at the 2:1 Fe^{2+}-to-protein ratio, when Yfh1 populates a trimeric state, there are two interaction interfaces between frataxin and the ferrochelatase dimer. Each interaction site involves one ferrochelatase monomer and one frataxin trimer, with conserved polar and charged amino acids of the two proteins positioned at hydrogen-bonding distances from each other. One of the subunits of the Yfh1 trimer interacts extensively with one subunit of the ferrochelatase dimer, contributing to the stability of the complex, whereas another trimer subunit is positioned for Fe^{2+} delivery. Single-turnover stopped-flow kinetics experiments demonstrate that increased rates of heme production result from monomers, dimers, and trimers, indicating that these forms are most efficient in delivering Fe^{2+} to ferrochelatase and sustaining porphyrin metalation. Furthermore, they support the proposal that frataxin-mediated delivery of this potentially toxic substrate overcomes formation of reactive oxygen species.

In an oxidative environment, like that of the mitochondrial matrix (1), free Fe^{2+} is rapidly oxidized to Fe^{3+} with the subsequent formation of insoluble $Fe(OH)_3$. This type of Fe^{2+} oxidation generally produces oxygen radicals. In addition, through the Fenton reaction in which Fe^{2+} reacts with hydrogen peroxide, highly toxic hydroxyl radicals are produced. Organisms have evolved mechanisms for the control of iron uptake, delivery, storage, and detoxification, including those for Fe^{2+} handling within mitochondria. Frataxin, a major mitochondrial protein player in this process, has a central role in iron detoxification and iron delivery in heme and iron-sulfur cluster (ISC)[5] synthesis (2–5) as well as in aconitase repair (6). Low levels of frataxin in humans are responsible for the progressive neurodegenerative disease Friedreich's ataxia, caused by trinucleotide repeat expansions in the first intron of the frataxin gene and the consequent gene silencing. Frataxin deficiency results in aberrations in cellular iron homeostasis, progressive accumulation of iron in mitochondria, high levels of oxidative stress, and deficiency in heme and ISC biosynthesis (4, 7–9).

Numerous studies focusing on human and *Saccharomyces cerevisiae* (Yfh1) frataxin (FXN) and their *Escherichia coli* ortholog, CyaY, showed the ability of this protein to bind different metal ions, among which are Fe^{2+} and Co^{2+} (10–15). Metal ion binding has been linked to the oligomerization propensity of yeast and bacterial frataxin, which can form oligomeric complexes with 3–24 or even 48 subunits (10, 11, 16–19). These oligomers and the oligomerization process have been studied using x-ray crystallography, electron microscopy (EM), and small angle x-ray scattering (SAXS) (18–21). Furthermore, the different oligomeric forms have been suggested to be associated with the different functions of frataxin (22).

The iron-dependent oligomerization is directly linked to iron detoxification through the frataxin-catalyzed ferroxidation

* This work was supported, in whole or in part, by National Institutes of Health Grant GM080270 (to G. C. F.). This work was also supported by a grant from the Swedish Research Council (Vetenskapsrådet) (to S. A.-K.) and the American Heart Association, Greater SE Affiliate, Grants 10GRNT4300073 and 13GRNT16970019 (to G. C. F.) and in part by National Institutes of Health Grant AG15709-19 (to G. I.) The authors declare that they have no conflicts of interest with the contents of this article. The content is solely the responsibility of the authors and does not necessarily represent the official views of the National Institutes of Health.

[S] This article contains supplemental Tables S1 and S2.

[1] Both authors contributed equally to the work.

[2] Present address: MAX IV Laboratory, Lund University, SE-22100 Lund, Sweden.

[3] To whom correspondence may be addressed: Dept. of Molecular Medicine, Morsani College of Medicine, MDC 7, University of South Florida, Tampa, FL 33612-4799. Tel.: 813-974-5797; Fax: 813-974-0504; E-mail: gferreir@health.usf.edu.

[4] To whom correspondence may be addressed. Tel.: 46733622978; E-mail: salam.al-karadaghi@biochemistry.lu.se.

[5] The abbreviations used are: ISC, iron-sulfur cluster; FXN, frataxin; Mfrn1, mitoferrin-1; BS^3, bis(sulfosuccinimidylsuberate).

reaction, in which two Fe^{2+} atoms are oxidized, whereas O_2 is reduced to O^{2-} (10, 11, 23–26). These events are followed by the formation of an insoluble ferrihydride iron core, similar in structure to the iron core of ferritin (21, 27). Frataxin's functional role as metal ion chaperone and direct Fe^{2+} donor to proteins have been substantiated in diverse experimental models (2, 6, 13, 28–31). Both human and yeast frataxin have been shown to deliver iron to the ISC scaffold protein (yeast Isu1/human ISCU) (29, 32), interacting with the sulfur donor, a cysteine desulfurase (yeast Nfs1/human NFS1, stabilized by Isd11/ISD11) during the synthesis of ISC cofactors. Frataxin has also been shown to interact with ferrochelatase and donate iron for heme synthesis (2, 11, 28). Ferrochelatase, the terminal enzyme of the heme biosynthesis pathway, catalyzes the insertion of Fe^{2+} into protoporphyrin IX (33). Frataxin-mediated iron delivery to ferrochelatase was supported by the initial observations that Yfh1-bound Fe^{2+} was not oxidized as readily as free Fe^{2+} in solution and that the transfer of Fe^{2+} from Yfh1 to ferrochelatase occurred even in presence of an excess of citrate, a physiological Fe^{2+} chelator, which suggested that direct protein-protein contacts and metal ligand exchange should take place (11, 24). In fact, Fe^{2+} could remain bound to Yfh1 for periods long enough to allow its delivery to the appropriate Fe^{2+} protein acceptors for either heme or ISC biosynthesis (11, 28, 29, 32).

Eukaryotic ferrochelatase is a homodimeric protein peripherally associated with the matrix side of the inner mitochondrial membrane. Although the physiological substrate of ferrochelatase is Fe^{2+}, the enzyme can also bind and catalyze the insertion of other divalent metal ions, such as Zn^{2+}, Ni^{2+}, Cu^{2+}, and Co^{2+}, into the porphyrin macrocycle (33). In 2006 it was proposed that due to its low metal ion specificity, ferrochelatase must rely on a metallochaperone (34). In early studies with Yfh1-deficient (Δ*yfh1*) *S. cerevisiae* cells, ferrochelatase was shown to catalyze the formation of zinc-protoporphyrin but not heme (28). These results demonstrated that, although catalytically competent, in the absence of frataxin ferrochelatase did not catalyze the insertion of Fe^{2+} into protoporphyrin. Nanomolar-range values for the binding constant (K_d) of frataxin and ferrochelatase, as measured using various biophysical approaches and proteins from different organisms (13, 28, 35), indicated a high affinity interaction between these two proteins. Specifically, surface plasmon resonance (Biacore) yielded a K_d of between 17 nM and 40 nM for the *in vitro* interaction between Yfh1 and yeast ferrochelatase (28), and similarly, isothermal titration calorimetry (ITC) returned a K_d of 1.7×10^{-8} M for the binding affinity of iron-loaded, mature truncated form of FXN (covering residues 81–210 (FXN^{81-210})) to human ferrochelatase (35). Moreover, *Bacillus subtilis* frataxin homolog, Fra, has been recently shown to interact with *B. subtilis* ferrochelatase HemH and to supply intracellularly Fe^{2+} to the enzyme for heme synthesis (36). Ferrochelatase-frataxin interaction was also corroborated with *in vitro* ferrochelatase activity assays in which oligomeric Yfh1 supported heme formation by providing iron to ferrochelatase at neutral pH in the presence of atmospheric oxygen and absence of reducing agents (11).

With the determination of the crystal structure of the 88–208 variant of human frataxin (FXN^{88-208}), Dhe-Paganon *et al.* (37) predicted that a conserved and predominantly hydrophobic region on the surface of the protein would mediate protein-protein interactions. Subsequently, Stemmler and coworkers (2, 13) by using nuclear magnetic resonance spectroscopy (NMR) identified frataxin helical plane as the possible ferrochelatase binding surface in the monomeric yeast Yfh1 and human FXN structures. However, the precise details of how Fe^{2+} is delivered to, or made available to ferrochelatase without being oxidized to Fe^{3+} remain to be defined. Zhang *et al.* (38), in teasing out the roles of *S. cerevisiae* mitochondrial carrier proteins Mrs3/Mrs4 and Yfh1, concluded that these proteins cooperate in supplying iron for heme synthesis; mrs3/4 carriers deliver iron into mitochondria, whereas Yfh1 makes iron bioavailable within mitochondria. A similar picture appears to be emerging from studies on mitochondrial iron metabolism in *Drosophila* (39, 40) and mammalian cells (41, 42).

In erythroblasts, the importer protein mitoferrin-1 (Mfrn1; Slc25a37) transports Fe^{2+} across the mitochondrial inner membrane (42–45). The complex of Mfrn1 with Abcb10 (an inner mitochondrial membrane ATP-binding cassette (ABC) transporter) increases Mfrn1 stability and enhances its half-life (46). Although Mfrn1 forms an immunoprecipitable complex with ferrochelatase (47), there is no evidence that Mfrn1 delivers Fe^{2+} to ferrochelatase. Due to the weak character of the interactions between ferrochelatase and Mfrn1, as suggested by the experiments, Chen *et al.* (47) proposed that the complex involving Mfrn1, Abcb10, and ferrochelatase could require additional (yet unidentified) bridging proteins.

Here we used presteady state kinetics to determine the rate of interaction between Yfh1 and ferrochelatase and the rate of ferrochelatase-catalyzed porphyrin metalation with either free Fe^{2+} or Fe^{2+}-bound Yfh1. The results support direct interaction between the proteins and are consistent with delivery of Fe^{2+} from Yfh1 to ferrochelatase, suggesting that the enhanced ferrochelatase activity stems from the Yfh1-promoted Fe^{2+} availability and direct supply to the enzyme. Single-particle reconstruction from negatively stained EM images was used to study the structure of the complex between ferrochelatase and frataxin. Protein-protein docking guided by cross-linking combined with mass-spectrometric analyses was used independently to create a quasi-atomic model of the complex between yeast ferrochelatase dimer and two Yfh1 trimers. This model was subsequently docked into the EM reconstruction and showed a good fit.

Experimental Procedures

Protein Expression, Purification, and Complex Preparation—The mature form of wild-type Yfh1 was expressed and purified as described previously (10). Mature yeast (*S. cerevisiae*) ferrochelatase was expressed as described for the murine enzyme in Ferreira (48) and purified according to the procedure in Ferreira *et al.* (49), with slight modifications to the composition of the buffers. The buffers and respective compositions were: lysis buffer (20 mM Tris-HCl, pH 8.0, containing 10% glycerol, 1.5% cholate, and 1.5 M sodium chloride), equilibration buffer (20

mM Tris-HCl, pH 8.0, containing 10% glycerol), wash buffer (20 mM Tris-HCl, pH 8.0, containing 10% glycerol and 1.5 M sodium chloride), and elution buffer (20 mM Tris-HCl, pH 8.0, containing 10% glycerol, 1.5 M sodium chloride, and 1.5% cholate).

Study of Protoporphyrin IX Binding to Ferrochelatase—The dissociation constant for the ferrochelatase-protoporphyrin IX complex was determined by direct spectrophotometric titration based on the loss of porphyrin fluorescence upon binding to the enzyme. A RF-5301 PC Shimadzu spectrofluorimeter was utilized, and the excitation wavelength was set to 407 nm, whereas the emission was recorded at 635 nm. A buffer solution containing 20 mM MOPS, pH 7.0, 0.4 M NaCl, 0.2% Tween 80, and 0.5 μM protoporphyrin IX was titrated incrementally with 93.2 μM yeast ferrochelatase, which was in a similar buffer but without protoporphyrin IX. The total volume of ferrochelatase added was <5% of the total volume and was not accounted for in the computations. The titration was run three times, and for each set of data the change in fluorescence was plotted as a function of ferrochelatase concentration. The points did not suggest cooperative binding and were fit to a quadratic equation (Equation 1) to determine the dissociation constant (Ref. 50, Equation II-53),

$$[ES] = \frac{\max([E]_0 + [S]_0 + K_d) \pm \sqrt{([E]_0 + [S]_0 + K_d)^2 - 4[E]_0[S]_0}}{2[S]_0} \quad \text{(Eq. 1)}$$

where [*ES*] represents the concentration of the enzyme-substrate complex, which is plotted at the *y* axis as the change in fluorescence, max refers to the fitted maximal percentage of quenching, $[E]_0$ is the initial enzyme concentration plotted at the *x* axis, $[S]_0$ represents the initial protoporphyrin IX concentration, which was 0.5 μM, K_d is the fitted dissociation constant.

Determination of the Rates of Frataxin-Ferrochelatase Association and Ferrochelatase-catalyzed Porphyrin Metalation by Stopped-flow UV-visible Spectroscopy—The presteady state kinetics of the association of Yfh1 and yeast ferrochelatase was examined by measuring changes in the intrinsic protein fluorescence intensity. Yfh1 and ferrochelatase, in 20 mM MOPS, pH 7.0, containing 0.4 M NaCl and 0.2% (v/v) Tween 80, were maintained at 20 °C in separate syringes before their mixing in the reaction chamber. The protein concentrations in the two syringes were 2-fold greater than the final concentrations in the reaction chamber (final concentrations are reported in Fig. 1 legend). The intrinsic protein fluorescence quenching was examined upon excitation at a wavelength of 280 nm. The emitted light was filtered using a 320-nm longpass filter placed over the photomultiplier detector. The time course data were fit to a single-exponential process (Equation 2),

$$\Delta F_{obs}(t) = A_1 e^{-k_{obs}t} + A_0 \quad \text{(Eq. 2)}$$

where $F_{obs}(t)$ is the observed fluorescence change (in arbitrary units) at time *t*, k_{obs} is the observed first-order rate constant, A_1 is the pre-exponential factor, and A_0 is the offset.

The rate for the ferrochelatase-catalyzed insertion of Fe^{2+} into protoporphyrin IX was monitored by following the decrease in protoporphyrin fluorescence intensity. The excitation wavelength was set to 407 nm, and a 520-nm longpass filter was used in the detection of the emitted light. The time course data were fit to Equation 2 as described above (the data were fit to a first-order exponential rather than a burst equation because the steady state rate was negligible or insignificant on this time scale, and the simpler equation facilitates a more precise determination of the burst rate, which is what the experiment was intended to measure). In addition, similar presteady state kinetic studies were performed in the presence and absence of EDTA, a strong metal ion chelator. All buffers were made with milliQ water, treated with the DIAION^{TM} CR11 (Sigma) metal ion-chelating resin, and filtered (0.2 μm) to remove metal ions.

Single-turnover Burst Kinetics of Ferrochelatase in the Absence and Presence of Frataxin—In all cases one of the two syringes contained 40 μM purified recombinant yeast frataxin (Yfh1) and 30 μM protoporphyrin IX. The dissociation constant for the yeast ferrochelatase-protoporphyrin complex was separately determined to be 0.29 ± 0.03 nM, indicating that under these conditions all of the porphyrin is bound to the enzyme. The other syringe contained 400 μM ferrous chloride and 0–300 μM Yfh1, as specifically indicated in the Fig. 1 legend. The buffer contained 20 mM MOPS, pH 7.0, 0.4 M NaCl, and 0.2% Tween 80. Before running the experiments, yeast ferrochelatase and Yfh1 were dialyzed into this buffer. The ferrochelatase-protoporphyrin syringe was prepared and loaded first, and Yfh1, when included, was added immediately after the ferrous chloride had been mixed into the buffer of the second syringe. Approximately 30 s elapsed between the time the ferrous chloride was added and the first trace was recorded.

Single-turnover Stopped-flow Experiments—All of the fluorescence stopped-flow experiments described in the following sections were conducted using a SF-2001 from KinTek Corp. The syringe and observation chambers were maintained at 20 °C with an external water bath, which approximately corresponded to room temperature at the time of the experiments. The photomultiplier detector was mounted at a right angle to the path of excitatory light entering the 0.2-cm^2 observation cell. For experiments monitoring the depletion of protoporphyrin IX, the excitation wavelength was set to 407 nm, and the photomultiplier was equipped with a 520-nm longpass filter.

Transmission Electron Microscopy—For preparation of the complex of ferrochelatase with frataxin trimers, Yfh1 at a concentration of 3 mg/ml (~22 μM) was incubated with ferrous ammonium sulfate at 2-to-1 iron-to-Yfh1 molar ratio for 60 min at 30 °C (19). This was followed by incubation of 1 part ferrochelatase (6 mg/ml) with 2 parts Yfh1 trimers (3 mg/ml) for 30 min at 30 °C, yielding a final protein concentration of 4 mg/ml (2 mg/ml Yfh1 and 2 mg/ml ferrochelatase). Reported protein molar concentrations are based on monomeric molecular masses of 13,783 and 41,209 daltons for Yfh1 and *S. cerevisiae* ferrochelatase, respectively, as calculated from the primary amino acid sequences encoded by the cDNAs for the two recombinant proteins.

The Yfh-ferrochelatase complex was applied to a 10/300 GL Superdex 200 gel filtration chromatography column (GE Healthcare) at a flow-rate of 0.5 ml/min and eluted at room temperature with HN100 buffer (20 mM HEPES, pH 7.3, and

100 mM NaCl) in 0.1-ml fractions. The recording was done at 280 nm (A_{280}).

Samples from fractions containing both Yfh1 and ferrochelatase (10 μl) were applied directly to a 400-mesh, carbon-coated, copper grid (Electron Microscopy Sciences) that had been preincubated for 1 min in HN100 buffer. After 1 min, excess protein sample was blotted with filter paper, and the grid was washed with sterile water for 3 s. Excess water was again removed by blotting. For staining, 1% (w/v) uranyl acetate was applied to the grid, and after 30 s excess stain was blotted. The grid was left to dry for ~30 min, after which it was inserted into the sample holder of a Philips CM120 transmission electron microscope equipped with a GATAN GIF 100 energy filter and a GATAN 791 CCD camera (1024 × 1024 pixels). Images were taken using 55,000× magnification, and image processing was performed with the EMAN2 software package (51). Classification of particles was made using six averaging iterations. 1184 particles were used for the final three-dimensional reconstruction, and a C2 point group symmetry was applied to the model. Validation of the final reconstructions was accomplished by comparing class averages with projections of the three-dimensional reconstructions in the same angular orientation. The resolution of the reconstruction was estimated to 38 Å. Chimera software was used to visualize the reconstruction (52).

Chemical Cross-linking, Proteolysis, and MALDI Mass Spectrometry—The Yfh1-ferrochelatase complex was cross-linked with a 1:1 mixture of H12:D12 isotopically labeled bis-(sulfosuccinimidylsuberate) (BS^3), a primary amine-specific chemical and cleavable cross-linker. The Yfh1-ferrochelatase complex sample (20 μl) was incubated with the BS^3 cross-linker in a 50:1 molar ratio of cross-linker:protein at 25 °C for 15 min. The reaction was quenched by adding Tris to a final concentration of 20 mM. Subsequently, the protein was precipitated with freeze-cold acetone, centrifuged, and resuspended in 50 mM ammonium bicarbonate buffer, pH 7.8. Endoproteinase GluC was used to digest the cross-linked Yfh1-ferrochelatase complex for 17 h at 37 °C. Because the Gluc endoproteinase, which cleaves the polypeptide C-terminal to glutamate residues, can also cleave C-terminal to aspartate residues, albeit at a 100–300 times slower rate, the GluC reaction time was the same for all experiments to ensure reproducibility in the results.

The GluC-cleaved peptide mixture was separated by reversed phase liquid chromatography and collected into 192 fractions on a MALDI target plate. Subsequently, the fractions were analyzed on a 4700 Proteomics Analyzer (Applied Biosystems/MDS SCIEX) as previously described (53). All mass spectrometry (MS) spectra were internally calibrated using internal calibration peptides added to the matrix, except in fractions where the ion suppression decreased the intensity of the calibration peptides. Data from MS and tandem MS (MS/MS) were analyzed with the program FINDX (53). FINDX is an in-house-developed software designed for detection of cross-linked peptides using isotope-labeled cross-linker and MALDI mass spectrometry. In contrast to other programs designed for use with high resolution electrospray instruments, where cross-link detection is based on acquisition of a large amount of high quality MS/MS data, FINDX is designed to select cross-linked peptides only based on MS data. Thus, in the primary data analysis, which is based on well calibrated MS data, cross-linked peptides are identified at a tolerance setting of 7 ppm as doublet peaks with the mass difference of 12.07573 Da (due to the incorporation of deuterium from the H12:D12 isotopically labeled BS^3). In the subsequent step the data are validated by acquiring MS/MS-data for the peaks that correspond to the suggested cross-links. The MS/MS-spectra are inspected manually and analyzed by the second module of FINDX, which considers the following matches: 1) the mass of the fragments cross-linked to the peptide (referred to as x-fragment) and 2) masses that match stepwise fragmentation peptides in the putative cross-linked peptide (referred to as sequence fragments). At this stage potential cross-links are confirmed with more than three x-fragments in the list of matched masses, with both parts of the cross-linker represented and with more than three sequence-fragments from each of the two cross-linked peptides. For this reason no statistics of MS/MS-data is provided by the FINDX report.

Protein-Protein Docking and Yfh1-Ferrochelatase Model Evaluation—Initial models (a total of 12,000) with randomized orientation of both docking partners in the complex between yeast frataxin Yfh1 trimer (PDB ID 3OEQ; Ref. 18) and yeast ferrochelatase (PDB ID 1LBQ; Ref. 20) were generated using the Rosetta 3.4 software package (54). The "low_res_protocol_only" docking flag in Rosetta was used during this stage. The initial models were filtered using distance constraints established from the results of the cross-linking experiments and sorted according to the Rosetta energy score. The Cα distance between two cross-linked lysines was set as <31.6 Å. This value was obtained after taking into account the length of the cross-linker spacer arm (11.4 Å) and the length of two lysine side chains (2 × 6.5 Å). In addition, estimates of the resolution-dependent error in the positions of the protein atoms of Yfh1 and ferrochelatase (5.1 Å and 2.1 Å, respectively) needed to be added. These were estimated at 3σ using Cruickshank's formula (55) rearranged by Blow (56). The single-particle reconstruction was converted from mrc format to a bead model in pdb format using the program EM2DAM from the ATSAS suite of programs (57). The program SUPCOMB (58) was then used to automatically fit the filtered, initial models from Rosetta to the bead model resulting from the EM reconstruction. All models that appeared to fit well to the reconstruction, as assessed by the scoring function of SUPCOMB and by manual inspection but in which the trimeric structures of Yfh1 would collide with the predicted position of the inner mitochondrial membrane, were removed. The remaining models (~2000) were taken for further refinement in Rosetta using the "docking_local_refine" as well as the standard "dock_pert 3 8" docking flags. The refined models were evaluated and sorted according to their interface score (the total score of the complex minus the total score of each partner in isolation, according to the Rosetta 3.4 manual).

Results

Transient Kinetic Analysis of Yfh1-mediated Fe^{2+} Transfer to Ferrochelatase—As shown previously with small angle x-ray scattering and x-ray crystallography, at a Fe^{2+}:Yfh1 ratio of 1:1

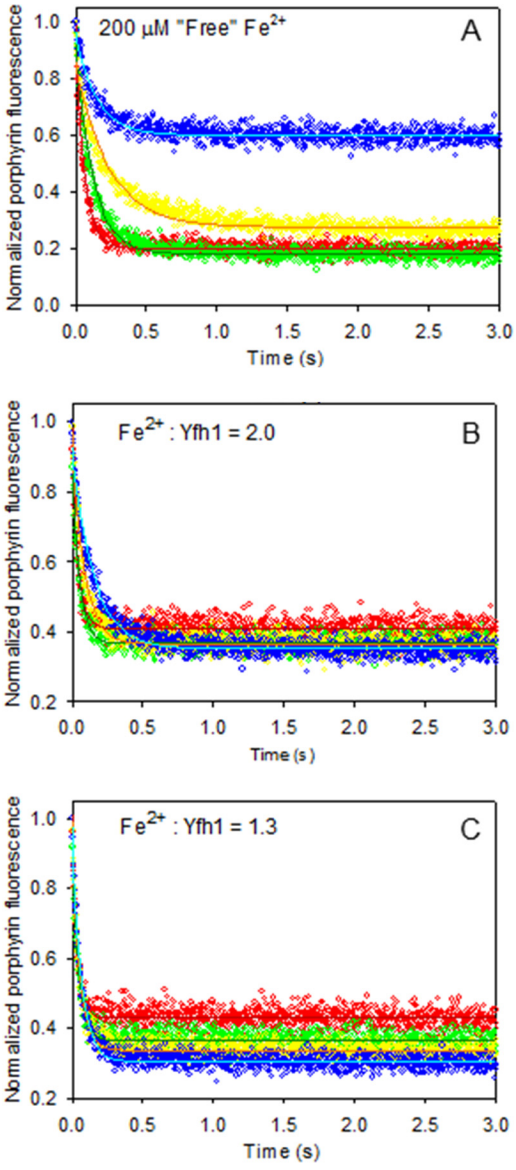

FIGURE 1. **Time dependence of heme synthesis at two Fe^{2+}:Yfh1 ratios.** Yeast ferrochelatase (20 μM) with bound protoporphyrin IX (15 μM) was mixed with 200 μM ferrous iron (*A*) in the absence of Yfh1 and in the presence of 100–200 μM Yfh1 (*B* and *C*). The Fe^{2+}:Yfh1 molar ratios were 2.0 (*B*) and 1.3 (*C*). In all cases, the *red*, *green*, *yellow*, and *blue circles* represent the kinetic traces at 0, 2, 5, and 10 min, respectively, after the initial shot (*i.e.* filling the stopped-flow syringes with the reactants).

Yfh1 populates a mixture of trimeric and monomeric states (38%/61% monomer/trimer), whereas at a ratio of and 2:1 the oligomeric state is predominantly trimeric (19). To determine if ferrochelatase-catalyzed heme synthesis depends on Fe^{2+} made available by Yfh1 and on the oligomeric state of Yfh1, single-turnover reactions were performed with Fe^{2+}:Yfh1 ratios of 0, 1.3, and 2.0. The rate of the reaction was monitored by following the consumption of the protoporphyrin IX substrate (or porphyrin metalation). The results show that in the absence of Yfh1 (Fig. 1*A*), the rate of the reaction was clearly slower than the reaction in the presence of Yhf1 at Fe^{2+}:Yfh1 ratios of 1.3 or 2 (Fig. 1, *B* and *C*) regardless of the "preincubation time" of Yfh1 with Fe^{2+} (different colored kinetic traces in Fig. 1, *B* and *C*). Furthermore, in the absence of Yhf1 (Fig. 1*A*) the rate of heme formation decreased with increasing the preincubation time (*yellow* and *blue circles* compared with *red* and *green* on Fig. 1*A*), presumably due to the oxidation of the "free" Fe^{2+} to Fe^{3+}, which is not a substrate of ferrochelatase. Higher Fe^{2+}:Yfh1 ratios (4, 7, and 10; data not shown), which result in higher order oligomers of frataxin, were also tested and showed dependence on incubation time similar to that of the Yfh1-free solution. This suggests that higher order frataxin oligomers, such as hexamers and dodecamers, etc., are less efficient in delivering iron to the ferrochelatase reaction. These results agree with our previous experiments performed under steady state conditions, which showed that at low Fe^{2+}:Yfh1 ratios, Fe^{2+} can be readily mobilized by chelators or made available to ferrochelatase to synthesize heme (11).

Rate of Yfh1-Ferrochelatase Association in Relation to the Rate of Heme Synthesis—To ascertain if the rate of complex formation between ferrochelatase and frataxin is consistent with direct transfer of Fe^{2+} from Yfh1 to ferrochelatase, we determined and compared the rates of association of Yfh1 with ferrochelatase and ferrochelatase-catalyzed Fe^{2+} insertion into protoporphyrin IX. The decrease in intrinsic protein fluorescence was used to follow the association of Yfh1 with ferrochelatase (*green circles* in Fig. 2*A*). The rate of complex formation was determined using transient (fluorescence stopped-flow spectroscopy) kinetics, which gave the value of $18 \pm 1\ s^{-1}$. The rate of the ferrochelatase-catalyzed metalation reaction was monitored by following the consumption of the protoporphyrin IX substrate (*red circles*, Fig. 2*A*), was $14.9 \pm 0.1\ s^{-1}$. The results show that the two proteins bind at a rate slightly faster than the rate of protoporphyrin IX metalation, in agreement with direct delivery of Fe^{2+} from Yfh1 to ferrochelatase.

We also performed transient kinetic studies of the ferrochelatase-catalyzed heme synthesis reaction using either free Fe^{2+} or Fe^{2+}-loaded Yfh1 in the presence and absence of EDTA. The addition of EDTA completely abolished heme production in the absence as well as in the presence of Yfh1, which was preincubated with Fe^{2+} at a Fe^{2+}-to-Yfh1 molar ratio of 2.5-to-1 (Fig. 2*B*). Although the reaction mechanism of Fe^{2+} dissociation from Yfh1 and Fe^{2+} association with and chelation by EDTA (*e.g.* formation of a ternary Fe(II)-Yfh1-ferrochelatase complex, scavenging of released Fe(II) from Yfh1 by EDTA yielding the EDTA-Fe(III) complex, or Fe(II) transfer between Yfh and ferrochelatase by a dissociative or an associative mechanism) is unknown, our findings indicates that EDTA, a strong chelator and catalyst of Fe(II) autooxidation, presumably "removes" Fe(II) from Yfh1 (59), rendering it in a form incompatible with its ferrochelatase-catalyzed insertion into protoporphyrin IX. These results are consistent with the observations showing a relatively low metal binding affinity by frataxin with dissociation constants in the micromolar range (2–3 μM; Refs. 13 and 14). Furthermore, the rate of heme synthesis was slightly accelerated when Fe^{2+} was provided from "Fe^{2+}-loaded Yfh1," in agreement with the chaperone role for Yfh1. It is important to note that protoporphyrin IX binds to ferrochelatase very tightly with a K_d value of 0.34 ± 0.04 μM under the conditions of these stopped-flow experiments (data not shown). This means that there is virtually no free protoporphy-

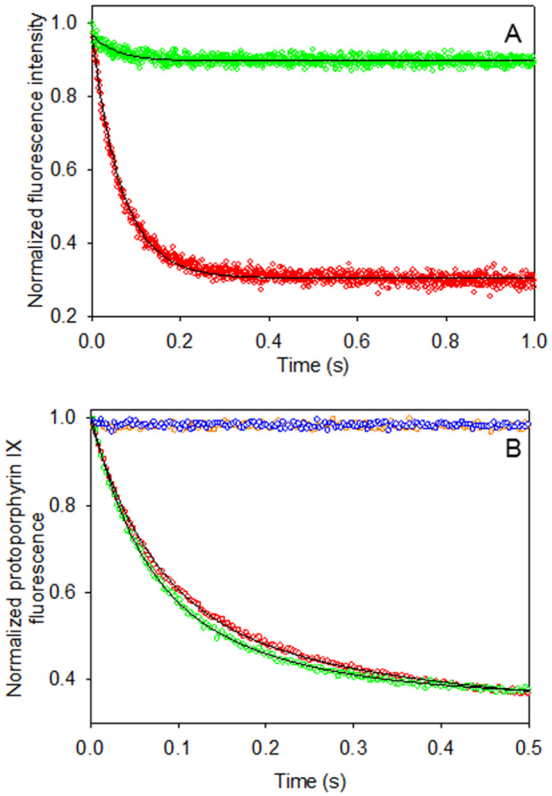

FIGURE 2. **Yfh1-mediated Fe^{2+} delivery to ferrochelatase.** *A*, the rate of ferrochelatase-Yfh1 association and ferrochelatase-catalyzed heme synthesis in the presence of Fe^{2+}-bound Yfh1. The decrease in intrinsic protein fluorescence was used to follow the association of Yfh1 with ferrochelatase (*green circles*); the rate of the ferrochelatase-catalyzed metalation reaction was monitored by following the consumption of the protoporphyrin IX substrate (*red circles*). Yeast ferrochelatase (10 μM) was mixed with 200 μM Yfh1–200 μM Fe^{2+} (final concentrations after mixing) in 20 mM MOPS, pH 7.0, containing 0.4 M NaCl and 0.2% (v/v) Tween 80. The observed rate constants were calculated by fitting the decrease in intrinsic protein fluorescence (*green circles*) or the decrease in protoporphyrin IX fluorescence (*red circles*) over time to Equation 2 for a single-exponential process. *B*, effects of Yfh1 and EDTA on the rate of heme synthesis by ferrochelatase. Yeast ferrochelatase (20 μM) incubated with protoporphyrin IX (15 μM) was mixed with 200 μM ferrous iron in the absence (*red circles*) or presence (80 μM; *green circles*) of Yfh1. In both cases the addition of EDTA at a concentration of 200 μM inhibited the reaction (*orange circles*, no Yfh1; *blue circles*, +Yfh1). Each trace represents the average of 10 experimental measurements. All concentrations given are the final concentrations in the observation chamber after mixing of the reactants.

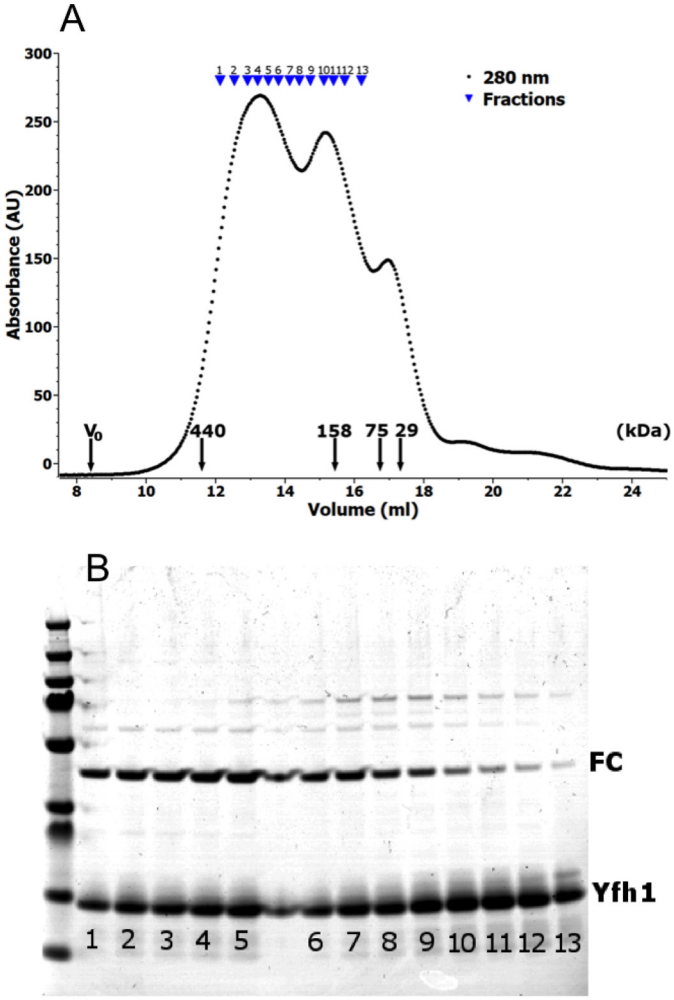

FIGURE 3. **Size exclusion chromatogram of the frataxin-ferrochelatase complex.** *A*, chromatogram of proteins eluted from the Superdex 200 resin as recorded at A_{280}. Fractions corresponding to the first two of the three peaks were run on SDS-PAGE (numbered *1–13*). Fractions from the second peak, primarily fraction no. 10, was used for transmission electron microscopy studies. *AU*, absorbance units. *B*, SDS-PAGE gel of fractions 1–13. The *first lane* contains protein markers. Ferrochelatase (44 kDa) indicated by *FC* and frataxin (14 kDa) by *Yfh1*.

rin IX present in solution, and it is, therefore, truly a single-turnover reaction (Fig. 2*B*).

EM Single-particle Reconstruction—Based on earlier gel-filtration studies,[6] which showed the formation of a complex between Yfh1 trimer and ferrochelatase, on the kinetic data obtained here on frataxin-ferrochelatase association and ferrochelatase-catalyzed porphyrin metalation and to ensure a homogenous complex, for the EM reconstruction it was decided to focus on the Fe^{2+}:Yfh1 ratio of 2:1. As mentioned above, at this ratio frataxin is expected to be primarily in the trimeric state. After formation (see "Experimental Procedures") the complex was applied to a gel filtration chromatography column. Sample analysis revealed three visible peaks corresponding to fractions containing proteins of approximate molecular mass of 240, 160, and 50 kDa (Fig. 3*A*). A small amount of sample from the fractions corresponding to the 160- and 240-kDa peaks was analyzed by SDS-PAGE (Fig. 3*B*) and protein staining. The analysis showed that the peaks contained both frataxin and ferrochelatase (Fig. 3*B*). Examination of negatively stained EM images of the fractions corresponding to the two peaks showed that the 240-kDa peak images contained mostly aggregated and irregular material, whereas the 160-kDa peak images together with other material contained repeating particles with recognizable shape (Fig. 4*A*). Furthermore, the apparent molecular mass of 160 kDa is very close to the molecular mass of a complex of 2 frataxin trimers with a ferrochelatase dimer (172 kDa). Thus, it was decided to use the images of the 160-kDa fractions for further analysis by single-particle reconstruction, as described under "Experimental Procedures." The complex was reconstructed using 1184 particles. Class averages of the collected particles and the final reconstructed volume are shown on Fig. 4*B* and Fig. 4, *C* and *D*, respectively. It should be noted that the complex was unstable under the conditions used to set up the grids, and presumably a large fraction of the pro-

[6] G. Isaya and O. Gakh, unpublished information.

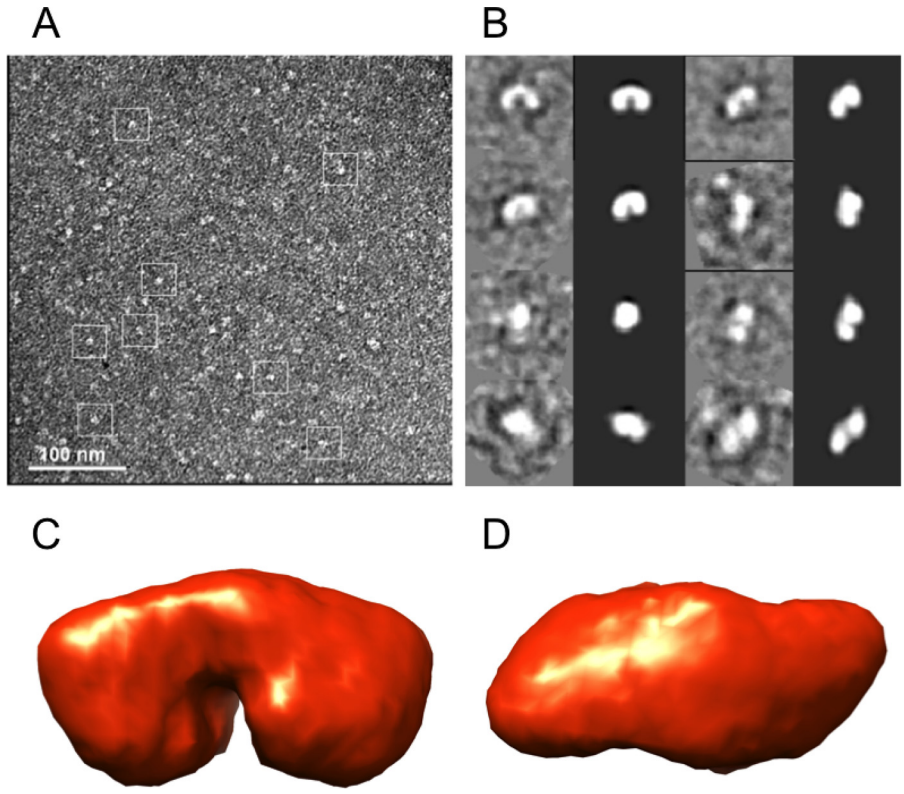

FIGURE 4. **EM reconstruction of the complex between yeast ferrochelatase and Yfh1.** *A*, an EM micrograph of the Yfh1-ferrochelatase complex. Particles chosen for the reconstruction are boxed. *B*, a comparison between projections of the single-particle reconstruction of the complex and the corresponding class averages. *C* and *D*, side (*B*) and top (*C*) view (looking down to the membrane) single-particle reconstruction of the complex between yeast ferrochelatase and Yfh1.

tein dissociated and aggregated after the addition of uranyl acetate and during grid preparation. Nevertheless, the number of collected particles allowed for the overall shape of the complex to be reconstructed. Using the EM volume and a combination of cross-linking, modeling, and docking of the x-ray structures of the frataxin trimer and yeast ferrochelatase dimer (see below), the reconstruction of the complex could be interpreted with one ferrochelatase dimer positioned in the center of the density flanked by two Yfh1 trimers bound on the sides, one trimer to each ferrochelatase subunit (Fig. 5, *A* and *B*, details presented below). The total buried surface area between the molecules was estimated to ~700 Å^2, which is within the range expected for transient molecular complexes.

Primary Amine-specific Cross-linking of the Complex between Yfh1 and Ferrochelatase—When the resolution of single-particle reconstructions from negatively stained EM images is not sufficient to unambiguously position high resolution structural models (from *e.g.* x-ray crystallography) into the reconstructed volume, distance constraints can be used to aid interpretation of the EM model. Here, we used primary amine-specific cross-linking of the Yfh1-ferrochelatase complex and, upon proteolysis with endoproteinase GluC, analyzed the cross-linked peptides by LC-MS and MS/MS. The established distance constraints were subsequently applied to filter the protein-protein docking simulations (see below).

Of several hundred masses, the FINDX software (53) identified four masses detected at 1565.77, 1621.90, 1638.80, and 2315.19 Da in the MS spectra with the 12-Da isotope doublet

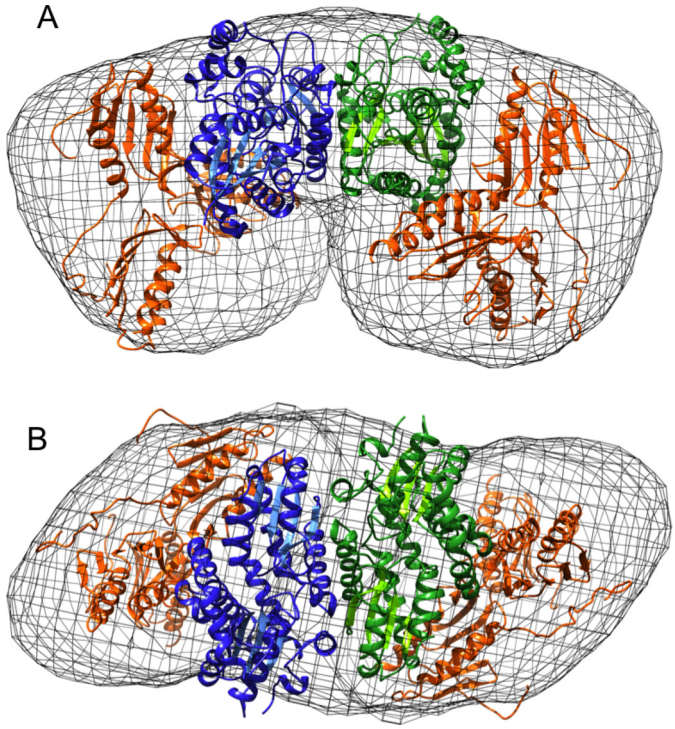

FIGURE 5. **The Rosetta model of the complex between yeast ferrochelatase and frataxin Yfh1 docked into the density generated from the single particle reconstruction.** The orientations in *A* and *B* are similar to those shown in Fig. 2, *B* and *C*. All structure figures were prepared using PyMOL (70).

peaks consistent with cross-linking between Yfh1 and ferrochelatase (supplemental Table S1). These four identified cross-linked Yfh1-ferrochelatase peptides were further analyzed by MS/MS, and two of them (with masses at 1565.77 Da and 1621.90 Da in MS) were verified by peptide sequencing supplemental Table S2) as described under "Experimental Procedures." From the determined cross-linked peptide sequences ^{72}KYHEE^{76} and ^{168}KAISKSQ^{174} of Yfh1 cross-linked to ^{93}KQYRE^{97} of ferrochelatase and with the theoretical masses of 1565.76 Da and 1621.89 Da, respectively, we found that either Lys-72 (from the flexible N terminus) or Lys-168/-172 (from the C-terminal helix) of Yfh1 were cross-linked to Lys-93 of ferrochelatase (Fig. 4*A*). Thus, and given the lengths of the BS^3 spacer arm and two lysine side chains (see "Experimental Procedures"), the Cα atom distances between Yfh1 Lys-72 and ferrochelatase Lys-93 and between Yfh1 Lys-168 (or Yfh1 K172) and ferrochelatase Lys-93 should be <31.6 Å.

Protein-Protein Docking Using Rosetta, EM, and Cross-linking—The initial model for the complex between ferrochelatase and frataxin was built using protein-protein docking and distance constraints acquired from the cross-linking studies without taking into account the EM reconstruction volume. Using the protein-protein docking program within the Rosetta package, 12,000 random complex models were created with the low resolution docking flag. Of these, 1269 fulfilled the distance constraints acquired from the cross-linking studies. These models were sorted according to the Rosetta energy score, and the top models were compared against the reconstructed EM volume. The two best-fit final models (model 1 and model 2) were chosen such that steric clashes between the frataxin subunits and the expected position of the mitochondrial membrane would be avoided. Subsequent fitting of the models to the EM reconstruction showed that model 1 could fit the EM reconstruction slightly better than model 2 (scores 3.738 and 3.820, respectively), whereas model 2 had a slightly lower Rosetta energy score (the lower the energy the better the model) compared with model 1 (−95.361 and −103.335 for models 1 and 2, respectively). Toward the final refinement we decided to produce 2000 refined models for each of models 1 and 2. The refined protein-protein docking resulted in complexes with similar fits to the reconstructed EM volume (scores 1.439 and 1.435 for models 1 and 2, respectively). However, the interface score (the total score of the complex minus the total score of each partner in isolation, according to the Rosetta 3.4 manual) was significantly better for refined model 1 compared with model 2 (4.27 and 2.37, respectively). Thus, model 1 was selected for the final evaluation of the complex.

Evaluation of the Model of Yfh1-Ferrochelatase Complex—Fig. 5*A* shows the refined model 1 of the complex between Yfh1 trimers and the ferrochelatase dimer superimposed on the EM reconstruction. In this model the relative orientation of the ferrochelatase dimer and the two frataxin trimers is such that the hydrophobic surface of ferrochelatase (facing the reader in Fig. 5*B*) faces the presumed membrane surface, where it is expected to receive the substrate, the highly hydrophobic protoporphyrin IX. This mode of interaction supports the physiological relevance of the model.

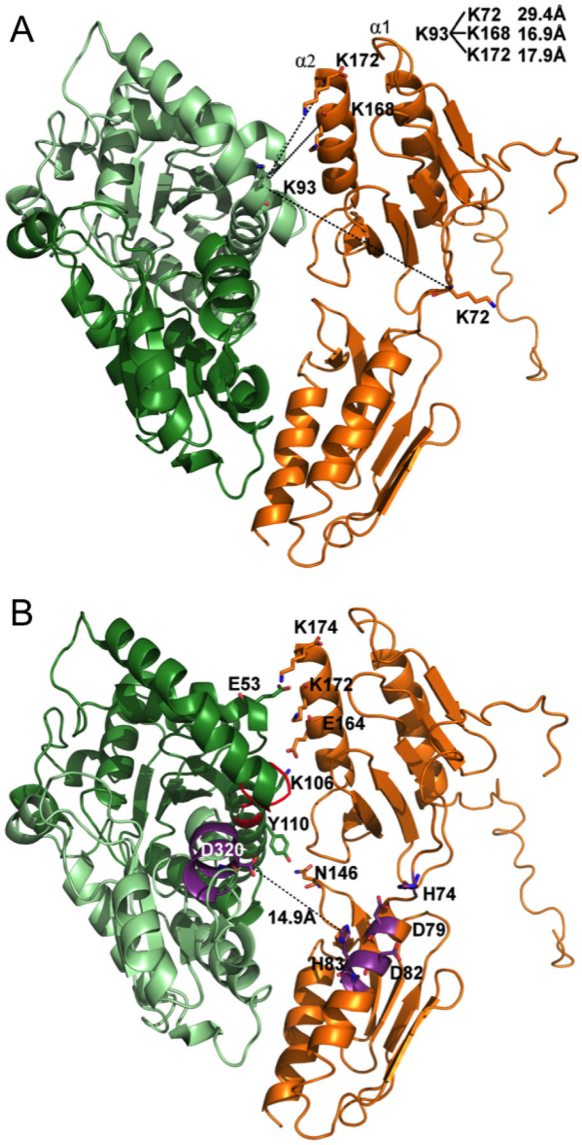

FIGURE 6. **Structural details of the complex between yeast ferrochelatase and frataxin Yfh1.** *A*, the cross-links between ferrochelatase (*green ribbon model*) and frataxin (*orange ribbon model*), which were analyzed in the MS experiments, are shown as *dotted lines*, and the corresponding amino acid side chains are shown in sticks representation. Only one ferrochelatase monomer is shown looking down into the porphyrin binding pocket. The cross-link distances between the amino acid residues involved in the cross-linking are shown in the insert. Only distance constrains obtained in the cross-linking experiments where used in the choice of the best model for docking into the EM density and for further analysis. Regions of frataxin helices α1 and α2, shown in NMR experiments (in which monomeric frataxin was used) to be involved in interactions with ferrochelatase, are colored in *magenta*. For clarity only two monomers of the frataxin trimer are shown on this figure. The third monomer points away from ferrochelatase and is not involved in complex formation. *B*, the side chains of frataxin and ferrochelatase amino acid residues involved in potential interactions within the complex are shown in sticks representation. A *dotted line* is drawn from the ferroxidation site of frataxin to Asp-320 of the π-helix of ferrochelatase, and the distance between the two sites is shown. Both regions are colored in *violet* for clarity. From the model it appears that although the upper frataxin monomer is involved in the stabilization of the complex, the lower monomer would deliver the metal to ferrochelatase.

Two monomers of the frataxin trimer appear to be positioned for interactions with a ferrochelatase monomer, whereas the third frataxin monomer does not contribute directly to the interactions (Fig. 6*A*). Several conserved ferrochelatase and

frataxin residues are located within the interaction surface area between Yfh1 and ferrochelatase (Fig. 6*B*). These include ferrochelatase residues from a loop between helices 2 and 3 (residues 98–103) and a conserved tryptophan (Trp-107). Residue Glu-97 together with His-317, which belongs to the π-helix of ferrochelatase (residues 313–325), have been shown earlier to bind Cd^{2+} in the yeast ferrochelatase structure (20). Conserved frataxin regions within the buried interface include residues from the end of the acidic α-helix (residues Glu-90 and Leu-91) as well as from the end of the second α-helix (Asn-154, Asp-160, and Glu-167). In an NMR spectroscopy study, which was limited to the use of frataxin monomers, most of the above-mentioned residues where shown to be affected by ferrochelatase-frataxin interactions (13). The present model also suggests potential hydrogen bonding interactions and salt bridges between Yfh1 and ferrochelatase. These include interactions between frataxin-ferrochelatase residues Asn-146–Tyr-110, Glu-164–Lys-106, and Lys-174–Glu-53 (Fig. 6*A*).

In our docked reconstruction of the complex between the frataxin trimers and the ferrochelatase dimer, the second frataxin monomer is positioned at a longer distance from the ferrochelatase monomer, too far for hydrogen bonding interactions to be formed. The residue His-83 from the ferroxidation site of Yfh1 is positioned at ~15 Å from the conserved Asp-320 of ferrochelatase (Fig. 4*B*); however, taking into account the low resolution of the model, this distance might be shorter or longer. Asp-320, like the above-mentioned His-317, is located in the π-helix, which connects the surface of the protein to the porphyrin binding cleft and the substrate metal ion binding site of ferrochelatase. The conserved acidic residues, aligned along the axis of the π-helix, have been proposed to constitute a route for Fe^{2+} transfer from the surface to the active site of the enzyme, where the metal ion is inserted into protoporphyrin IX (60). Thus, it is plausible that although one of the frataxin monomers is involved in extensive complex-stabilizing interactions, the second monomer is positioned for Fe^{2+} delivery to ferrochelatase.

It should be noted that the focus on the complex of frataxin trimer with ferrochelatase does not exclude the presence of other types of complexes in the images, for example complexes of ferrochelatase with monomers and dimers of frataxin. However, these would be difficult to clearly separate on the images for the sake of a separate single-particle reconstruction.

Discussion

In this work we present a structural model of the complex between yeast frataxin trimers and yeast ferrochelatase and show that the rate of heme production by ferrochelatase is dependent on the type of Yfh1 oligomers present in solution. In particular, when compared with free Fe^{2+}, the rate of heme production is higher in the presence of monomers and trimer and is reduced in the presence of larger Yfh1 oligomers, like hexamers and 24-mers. Earlier, Park *et al.* (11) showed that Yfh1 could bind large quantities of iron, keeping it available for ferrochelatase during long time periods. The authors also showed that iron sequestered inside larger Yfh1 oligomers, like 24-mers, was less accessible to the ferrochelatase reaction. It should be noted that although iron:frataxin ratios higher than 2:1 trigger the formation of oligomers of order higher than trimers, they also reduce the percentage of available monomers and trimers (19), which as shown here are the most favorable forms of frataxin for iron delivery to ferrochelatase.

It is of interest to compare the mechanisms of the chaperone function of frataxin with those of the better-studied copper chaperone system. Similar to iron, copper supports redox chemistry in cells and, if unrestrained, can be highly toxic for organisms (61). The best-studied copper chaperone Atx1 appears to protect Cu(I) from nonspecific reactions, allowing rapid metal transfer to its partners (62). This process is believed to proceed through substitution of metal ligands on the donor chaperone by new ligands from the acceptor target protein after the formation of a complex between the proteins (61, 63). Weak, transient protein-protein interactions have been shown to form the basis for complex formation (64). Moreover, it has been shown that copper ion is necessary for the formation of the complex between Atx1 and Ccc2 ATPase and that no interaction occurs between the apo-forms of the proteins (63).

The structure of the complex of ferrochelatase and frataxin presented here suggests that both proteins are engaged in close interactions with each other, creating a route for Fe^{2+} transfer from the metal binding site of frataxin to the site of the ferrochelatase reaction. This route appears to involve the π-helix of ferrochelatase, a conserved structural element that contains several acidic residues aligned along the helix axis. Only a π-helix may provide such alignment of amino acid side chains along the helix axis (65).

The results also support earlier work in which different experimental methods used to study the interactions between ferrochelatase and frataxin clearly pointed to the existence of direct contacts between the two proteins (11, 13, 28, 35, 38, 47), although the precise oligomeric state of frataxin required for the most favorable interaction was not discussed. In the presented model of the complex between yeast ferrochelatase and Yfh1, His-83 of the ferroxidation site of frataxin, believed to be one of the iron binding residues, is around 15 Å away from Asp-320 of the π-helix of ferrochelatase (Fig. 4*B*). This distance could be too long for direct ligand exchange to take place, but taken into account the low resolution of the structure and the transient character of the complex, closer interactions between the two sites, which would include frataxin His-83, and ferrochelatase Asp-320 and possibly His-317 (previously shown to bind cadmium) are feasible in solution. Although in solution, Fe^{2+} is normally coordinated by six water molecules, Fe^{2+} at the di-iron ferroxidation site of frataxin, similarly to ferritin, may be coordinated to a histidine and acidic amino acid residues as well as to water (66, 67). The water molecule could take part in ligand exchange by being initially replaced by one of the acidic residues of the π-helix of ferrochelatase. Partial dehydration of the iron before arriving at the ferrochelatase active center histidine and glutamate residues would facilitate the reaction of iron insertion into protoporphyrin IX (68).

Under experimental conditions favoring the formation of Yfh1 trimers, the rate of complex formation between Yfh1 and

ferrochelatase is slightly faster than that of heme formation ($18 \pm 1\ s^{-1}$ *versus* $14.9 \pm 0.1\ s^{-1}$). This is consistent with the idea that a step involving complex formation takes place before porphyrin metalation. Furthermore, Fe^{2+} needs to be loosely bound to Yfh1 for a delivery process to be efficient. The fact that EDTA inhibits porphyrin metalation in the presence of Yfh1 indicates that EDTA binds the metal ion much more tightly than the protein, which has instead evolved to chaperone the metal ion. In prior steady state kinetic experiments we postulated that if Yfh1-bound Fe^{2+} is not transferred to a ligand (*e.g.* ferrochelatase), its oxidation and mineralization proceed to completion, with Fe^{3+} becoming progressively less accessible, being sequestered within the iron core of frataxin (11). Although other Fe^{2+} chaperones cannot be ruled out as donors of the metal substrate to ferrochelatase, frataxin appears to meet the structural and functional requirements for such a role. Moreover, recently, Mielcarek *et al.* (36) reported that the physical interaction between the *B. subtilis* homologs of frataxin and ferrochelatase (hemH) mediated Fe^{2+} supply and sustained heme biosynthesis *in vivo*. A similar scenario is very likely in yeast and other eukaryotes. Conceivably, in the erythroblast, the inner mitochondrial transporter Mfrn1 (69), frataxin, and ferrochelatase may form a dynamic and transient complex, and at different times the complex could also include other protein partners. According to this model, Mfrn1 may import Fe^{2+} across the inner mitochondrial membrane and frataxin chaperones and delivers Fe^{2+} to ferrochelatase. The model corroborates the cooperative roles observed for the yeast Mfrn ortholog mrs3/4 and yeast frataxin Yfh1 (38) and the need for the proposed bridging proteins stabilizing the immunoprecipitable Mfrn1-ferrochelatase complex (47). In sum, a stable multicomponent complex with at least the ferrochelatase dimer and two frataxin trimers as protein partners would serve two important purposes: 1) to enable the protected delivery of potentially toxic Fe^{2+} to ferrochelatase and 2) to enable the specificity of ferrochelatase for Fe^{2+} over other divalent metal ions and thus heme synthesis under physiological conditions.

Author Contributions—S. A.-K., G. C. F., and G. I. conceived and coordinated the study, contributed to the analysis of the data, and wrote the paper. C. S. designed, performed, and analyzed the EM study, docking, cross-linking, and mass spectrometric analysis. M. E. G. designed, performed, and analyzed the kinetic experiments shown in Figs. 1 and 2. E.-C. A. provided technical assistance in sample preparation for EM, EM data collection, and processing. G. A. H. and O. G. provided technical assistance and contributed to the preparation of the manuscript. All authors reviewed the results and approved the final version of the manuscript.

References

1. Hu, J., Dong, L., and Outten, C. E. (2008) The redox environment in the mitochondrial intermembrane space is maintained separately from the cytosol and matrix. *J. Biol. Chem.* **283,** 29126–29134
2. Bencze, K. Z., Yoon, T., Millan-Pacheco, C., Bradley, P. B., Pastor, N., Cowan, J. A., and Stemmler, T. L. (2007) Human frataxin: iron and ferrochelatase binding surface. *Chem. Comm.* **18,** 1798–1800
3. Rawat, S., and Stemmler, T. L. (2011) Key players and their role during mitochondrial iron-sulfur cluster biosynthesis. *Chemistry* **17,** 746–753
4. Vaubel, R. A., and Isaya, G. (2013) Iron-sulfur cluster synthesis, iron homeostasis and oxidative stress in Friedreich ataxia. *Mol. Cell Neurosci.* **55,** 50–61
5. Pastore, A., and Puccio, H. (2013) Frataxin: a protein in search for a function. *J. Neurochem.* **126,** 43–52
6. Bulteau, A. L., O'Neill, H. A., Kennedy, M. C., Ikeda-Saito, M., Isaya, G., and Szweda, L. I. (2004) Frataxin acts as an iron chaperone protein to modulate mitochondrial aconitase activity. *Science* **305,** 242–245
7. Isaya, G. (2014) Mitochondrial iron-sulfur cluster dysfunction in neurodegenerative disease. *Front. Pharmacol.* **5,** 29
8. Hadzhieva, M., Kirches, E., and Mawrin, C. (2014) Review: iron metabolism and the role of iron in neurodegenerative disorders. *Neuropathol. Appl. Neurobiol.* **40,** 240–257
9. Abrahão, A., Pedroso, J. L., Braga-Neto, P., Bor-Seng-Shu, E., de Carvalho Aguiar, P., and Barsottini, O. G. (2015) Milestones in Friedreich ataxia: more than a century and still learning. *Neurogenetics* **16,** 151–160
10. Gakh, O., Adamec, J., Gacy, A. M., Twesten, R. D., Owen, W. G., and Isaya, G. (2002) Physical evidence that yeast frataxin is an iron storage protein. *Biochemistry* **41,** 6798–6804
11. Park, S., Gakh, O., O'Neill, H. A., Mangravita, A., Nichol, H., Ferreira, G. C., and Isaya, G. (2003) Yeast frataxin sequentially chaperones and stores iron by coupling protein assembly with iron oxidation. *J. Biol. Chem.* **278,** 31340–31351
12. Nair, M., Adinolfi, S., Pastore, C., Kelly, G., Temussi, P., and Pastore, A. (2004) Solution structure of the bacterial frataxin ortholog, CyaY: mapping the iron binding sites. *Structure* **12,** 2037–2048
13. He, Y., Alam, S. L., Proteasa, S. V., Zhang, Y., Lesuisse, E., Dancis, A., and Stemmler, T. L. (2004) Yeast frataxin solution structure, iron binding, and ferrochelatase interaction. *Biochemistry* **43,** 16254–16262
14. Cook, J. D., Bencze, K. Z., Jankovic, A. D., Crater, A. K., Busch, C. N., Bradley, P. B., Stemmler, A. J., Spaller, M. R., and Stemmler, T. L. (2006) Monomeric yeast frataxin is an iron-binding protein. *Biochemistry* **45,** 7767–7777
15. Pastore, C., Franzese, M., Sica, F., Temussi, P., and Pastore, A. (2007) Understanding the binding properties of an unusual metal-binding protein: a study of bacterial frataxin. *FEBS J.* **274,** 4199–4210
16. Adamec, J., Rusnak, F., Owen, W. G., Naylor, S., Benson, L. M., Gacy, A. M., and Isaya, G. (2000) Iron-dependent self-assembly of recombinant yeast frataxin: implications for Friedreich ataxia. *Am. J. Hum. Genet.* **67,** 549–562
17. Cavadini, P., O'Neill, H. A., Benada, O., and Isaya, G. (2002) Assembly and iron-binding properties of human frataxin, the protein deficient in Friedreich ataxia. *Hum. Mol. Genet.* **11,** 217–227
18. Söderberg, C. A., Shkumatov, A. V., Rajan, S., Gakh, O., Svergun, D. I., Isaya, G., and Al-Karadaghi, S. (2011) Oligomerization propensity and flexibility of yeast frataxin studied by x-ray crystallography and small-angle x-ray scattering. *J. Mol. Biol.* **414,** 783–797
19. Söderberg, C. A., Rajan, S., Shkumatov, A. V., Gakh, O., Schaefer, S., Ahlgren, E. C., Svergun, D. I., Isaya, G., and Al-Karadaghi, S. (2013) The molecular basis of iron-induced oligomerization of frataxin and the role of the ferroxidation reaction in oligomerization. *J. Biol. Chem.* **288,** 8156–8167
20. Karlberg, T., Schagerlöf, U., Gakh, O., Park, S., Ryde, U., Lindahl, M., Leath, K., Garman, E., Isaya, G., and Al-Karadaghi, S. (2006) The structures of frataxin oligomers reveal the mechanism for the delivery and detoxification of iron. *Structure* **14,** 1535–1546
21. Schagerlöf, U., Elmlund, H., Gakh, O., Nordlund, G., Hebert, H., Lindahl, M., Isaya, G., and Al-Karadaghi, S. (2008) Structural basis of the iron storage function of frataxin from single-particle reconstruction of the iron-loaded oligomer. *Biochemistry* **47,** 4948–4954
22. O'Neill, H. A., Gakh, O., and Isaya, G. (2005) Supramolecular assemblies of human frataxin are formed via subunit-subunit interactions mediated by a non-conserved amino-terminal region. *J. Mol. Biol.* **345,** 433–439
23. Adamec, J., Rusnak, F., Owen, W. G., Naylor, S., Benson, L. M., Gacy, A. M., and Isaya, G. (2000) Iron-dependent self-assembly of recombinant yeast frataxin: implications for Friedreich ataxia. *Am. J. Hum. Genet.* **67,** 549–562
24. Park, S., Gakh, O., Mooney, S. M., and Isaya, G. (2002) The ferroxidase

activity of yeast frataxin. *J. Biol. Chem.* **277,** 38589–38595
25. O'Neill, H. A., Gakh, O., Park, S., Cui, J., Mooney, S. M., Sampson, M., Ferreira, G. C., and Isaya, G. (2005) Assembly of human frataxin is a mechanism for detoxifying redox-active iron. *Biochemistry* **44,** 537–545
26. Gakh, O., Park, S., Liu, G., Macomber, L., Imlay, J. A., Ferreira, G. C., and Isaya, G. (2006) Mitochondrial iron detoxification is a primary function of frataxin that limits oxidative damage and preserves cell longevity. *Hum. Mol. Genet.* **15,** 467–479
27. Nichol, H., Gakh, O., O'Neill, H. A., Pickering, I. J., Isaya, G., and George, G. N. (2003) Structure of frataxin iron cores: an x-ray absorption spectroscopic study. *Biochemistry* **42,** 5971–5976
28. Lesuisse, E., Santos, R., Matzanke, B. F., Knight, S. A., Camadro, J. M., and Dancis, A. (2003) Iron use for haeme synthesis is under control of the yeast frataxin homologue (Yfh1). *Hum. Mol. Genet.* **12,** 879–889
29. Yoon, T., and Cowan, J. A. (2003) Iron-sulfur cluster biosynthesis. Characterization of frataxin as an iron donor for assembly of [2Fe-2S] clusters in ISU-type proteins. *J. Am. Chem. Soc.* **125,** 6078–6084
30. Gakh, O., Bedekovics, T., Duncan, S. F., Smith, D. Y., 4th, Berkholz, D. S., and Isaya, G. (2010) Normal and Friedreich ataxia cells express different isoforms of frataxin with complementary roles in iron-sulfur cluster assembly. *J. Biol. Chem.* **285,** 38486–38501
31. Maliandi, M. V., Busi, M. V., Turowski, V. R., Leaden, L., Araya, A., and Gomez-Casati, D. F. (2011) The mitochondrial protein frataxin is essential for heme biosynthesis in plants. *FEBS J.* **278,** 470–481
32. Li, H., Gakh, O., Smith, D. Y., 4th, and Isaya, G. (2009) Oligomeric yeast frataxin drives assembly of core machinery for mitochondrial iron-sulfur cluster synthesis. *J. Biol. Chem.* **284,** 21971–21980
33. Ferreira, G. C., and Hunter, G. A. (2011) Ferrochelatase structure and reaction mechanism. In *Handbook of Porphyrin Science with Applications to Chemistry, Physics, Materials Science, Engineering, Biology and Medicine*, *Biochemistry of Tetrapyrroles* (Kadish, K. M., Smith, K. M., and Guilard, R., eds) Vol. 15, pp. 49–121, World Scientific Publishing Co., Singapore
34. Al-Karadaghi, S., Franco, R., Hansson, M., Shelnutt, J. A., Isaya, G., and Ferreira, G. C. (2006) Chelatases: distort to select? *Trends Biochem. Sci.* **31,** 135–142
35. Yoon, T., and Cowan, J. A. (2004) Frataxin-mediated iron delivery to ferrochelatase in the final step of heme biosynthesis. *J. Biol. Chem.* **279,** 25943–25946
36. Mielcarek, A., Blauenburg, B., Miethke, M., and Marahiel, M. A. (2015) Molecular insights into frataxin-mediated iron supply for heme biosynthesis in *Bacillus subtilis*. *PLoS ONE* **10,** e0122538
37. Dhe-Paganon, S., Shigeta, R., Chi, Y. I., Ristow, M., and Shoelson, S. E. (2000) Crystal structure of human frataxin. *J. Biol. Chem.* **275,** 30753–30756
38. Zhang, Y., Lyver, E. R., Knight, S. A., Lesuisse, E., and Dancis, A. (2005) Frataxin and mitochondrial carrier proteins, Mrs3p and Mrs4p, cooperate in providing iron for heme synthesis. *J. Biol. Chem.* **280,** 19794–19807
39. Hales, K. G. (2010) Iron testes: sperm mitochondria as a context for dissecting iron metabolism. *BMC Biol.* **8,** 79
40. Metzendorf, C., and Lind, M. I. (2010) Drosophila mitoferrin is essential for male fertility: evidence for a role of mitochondrial iron metabolism during spermatogenesis. *BMC Dev. Biol.* **10,** 68
41. Richardson, D. R., Huang, M. L., Whitnall, M., Becker, E. M., Ponka, P., and Suryo Rahmanto, Y. (2010) The ins and outs of mitochondrial iron-loading: the metabolic defect in Friedreich's ataxia. *J. Mol. Med.* **88,** 323–329
42. Richardson, D. R., Lane, D. J., Becker, E. M., Huang, M. L., Whitnall, M., Suryo Rahmanto, Y., Sheftel, A. D., and Ponka, P. (2010) Mitochondrial iron trafficking and the integration of iron metabolism between the mitochondrion and cytosol. *Proc. Natl. Acad. Sci. U.S.A.* **107,** 10775–10782
43. Shaw, P., Greenstein, D., Lerch, J., Clasen, L., Lenroot, R., Gogtay, N., Evans, A., Rapoport, J., and Giedd, J. (2006) Intellectual ability and cortical development in children and adolescents. *Nature* **440,** 676–679
44. Paradkar, P. N., Zumbrennen, K. B., Paw, B. H., Ward, D. M., and Kaplan, J. (2009) Regulation of mitochondrial iron import through differential turnover of mitoferrin 1 and mitoferrin 2. *Mol. Cell. Biol.* **29,** 1007–1016
45. Schultz, I. J., Chen, C., Paw, B. H., and Hamza, I. (2010) Iron and porphyrin trafficking in heme biogenesis. *J. Biol. Chem.* **285,** 26753–26759
46. Chen, W., Paradkar, P. N., Li, L., Pierce, E. L., Langer, N. B., Takahashi-Makise, N., Hyde, B. B., Shirihai, O. S., Ward, D. M., Kaplan, J., and Paw, B. H. (2009) Abcb10 physically interacts with mitoferrin-1 (Slc25a37) to enhance its stability and function in the erythroid mitochondria. *Proc. Natl. Acad. Sci. U.S.A.* **106,** 16263–16268
47. Chen, W., Dailey, H. A., and Paw, B. H. (2010) Ferrochelatase forms an oligomeric complex with mitoferrin-1 and Abcb10 for erythroid heme biosynthesis. *Blood* **116,** 628–630
48. Ferreira, G. C. (1994) Mammalian ferrochelatase. Overexpression in *Escherichia coli* as a soluble protein, purification and characterization. *J. Biol. Chem.* **269,** 4396–4400
49. Hunter, G. A., Sampson, M. P., and Ferreira, G. C. (2008) Metal ion substrate inhibition of ferrochelatase. *J. Biol. Chem.* **283,** 23685–23691
50. Segel, I. H. (1993) *Enzyme Kinetics: Behavior and Analysis of Rapid Equilibrium and Steady State Enzyme Systems*, pp. 18–99, John Wiley & Sons, Inc., New York
51. Tang, G., Peng, L., Baldwin, P. R., Mann, D. S., Jiang, W., Rees, I., and Ludtke, S. J. (2007) EMAN2: an extensible image processing suite for electron microscopy. *J. Struct. Biol.* **157,** 38–46
52. Pettersen, E. F., Goddard, T. D., Huang, C. C., Couch, G. S., Greenblatt, D. M., Meng, E. C., and Ferrin, T. E. (2004) UCSF Chimera: a visualization system for exploratory research and analysis. *J. Comput. Chem.* **25,** 1605–1612
53. Söderberg, C. A., Lambert, W., Kjellström, S., Wiegandt, A., Wulff, R. P., Månsson, C., Rutsdottir, G., and Emanuelsson, C. (2012) Detection of crosslinks within and between proteins by LC-MALDI-TOFTOF and the software FINDX to reduce the MSMS-data to acquire for validation. *PLoS ONE* **7,** e38927
54. Leaver-Fay, A., Tyka, M., Lewis, S. M., Lange, O. F., Thompson, J., Jacak, R., Kaufman, K., Renfrew, P. D., Smith, C. A., Sheffler, W., Davis, I. W., Cooper, S., Treuille, A., Mandell, D. J., Richter, F., *et al.* (2011) ROSETTA3: an object-oriented software suite for the simulation and design of macromolecules. *Methods Enzymol.* **487,** 545–574
55. Cruickshank, D. W. (1999) Remarks about protein structure precision. *Acta Crystallogr. D Biol. Crystallogr.* **55,** 583–601
56. Blow, D. M. (2002) Rearrangement of Cruickshank's formulae for the diffraction-component precision index. *Acta Crystallogr. D Biol. Crystallogr.* **58,** 792–797
57. Petoukhov, M. V., Franke, D., Shkumatov, A. V., Tria, G., Kikhney, A. G., Gajda, M., Gorba, C., Mertens, H. D., Konarev, P. V., and Svergun, D. I. (2012) New developments in the program package for small-angle scattering data analysis. *J. Appl. Crystallogr.* **45,** 342–350
58. Kozin, M. B., and Svergun, D. I. (2001) Automated matching of high- and low-resolution structural models. *J. Appl. Cryst.* **34,** 33–41
59. Welch, K. D., Davis, T. Z., and Aust, S. D. (2002) Iron autoxidation and free radical generation: effects of buffers, ligands, and chelators. *Arch. Biochem. Biophys.* **397,** 360–369
60. Lecerof, D., Fodje, M. N., Alvarez León, R., Olsson, U., Hansson, A., Sigfridsson, E., Ryde, U., Hansson, M., and Al-Karadaghi, S. (2003) Metal binding to *Bacillus subtilis* ferrochelatase and interaction between metal sites. *J. Biol. Inorg. Chem.* **8,** 452–458
61. Pufahl, R. A., Singer, C. P., Peariso, K. L., Lin, S. J., Schmidt, P. J., Fahrni, C. J., Culotta, V. C., Penner-Hahn, J. E., and O'Halloran, T. V. (1997) Metal ion chaperone function of the soluble Cu(I) receptor Atx1. *Science* **278,** 853–856
62. Huffman, D. L., and O'Halloran, T. V. (2000) Energetics of copper trafficking between the Atx1 metallochaperone and the intracellular copper transporter, Ccc2. *J. Biol. Chem.* **275,** 18611–18614
63. Banci, L., Bertini, I., Cantini, F., Felli, I. C., Gonnelli, L., Hadjiliadis, N., Pierattelli, R., Rosato, A., and Voulgaris, P. (2006) The Atx1-Ccc2 complex is a metal-mediated protein-protein interaction. *Nat. Chem. Biol.* **2,** 367–368
64. Robinson, N. J., and Winge, D. R. (2010) Copper metallochaperones. *Annu. Rev. Biochem.* **79,** 537–562
65. Fodje, M. N., and Al-Karadaghi, S. (2002) Occurrence, conformational

features and amino acid propensities for the pi-helix. *Protein Eng.* **15,** 353–358
66. Hempstead, P. D., Hudson, A. J., Artymiuk, P. J., Andrews, S. C., Banfield, M. J., Guest, J. R., and Harrison, P. M. (1994) Direct observation of the iron binding sites in a ferritin. *FEBS Lett.* **350,** 258–262
67. Arosio, P., Ingrassia, R., and Cavadini, P. (2009) Ferritins: a family of molecules for iron storage, antioxidation, and more. *Biochim. Biophys. Acta* **1790,** 589–599
68. Shen, Y., and Ryde, U. (2005) Reaction mechanism of porphyrin metallation studied by theoretical methods. *Chemistry* **11,** 1549–1564
69. Shaw, G. C., Cope, J. J., Li, L., Corson, K., Hersey, C., Ackermann, G. E., Gwynn, B., Lambert, A. J., Wingert, R. A., Traver, D., Trede, N. S., Barut, B. A., Zhou, Y., Minet, E., Donovan, A., Brownlie, A., Balzan, R., Weiss, M. J., Peters, L. L., Kaplan, J., Zon, L. I., and Paw, B. H. (2006) Mitoferrin is essential for erythroid iron assimilation. *Nature* **440,** 96–100
70. DeLano, W. L. (2010) *The PyMOL Molecular Graphics System*, Version 1.3r1, Schrodinger, LLC, New York